Journal of Computational Applied Mechanics 2026, 57(2): 257-274

DOI: 10.22059/jcamech.2025.408569.1746

RESEARCH PAPER

Vibration Analysis of Stiffened Composite Plates Reinforced by Nano materials: Analytical and Experimental Investigations

Adwaa M. Abdulmajeed [a], Emad Kadum Njim [b,*] , Firas Thair Al-Maliky [c], Royal Madan [d]

[a] *Department of Prosthetics and Orthotic Devices Engineering, Techniques College of Medical Rehabilitation and Prosthetics, Al-Furat Al-Awsat Technical University, Najaf, Iraq*

[b] *Ministry of Industry and Minerals, State Company for Rubber and Tires Industries, Najaf, 00964, Iraq*

[c] *Fuel and Energy Techniques Engineering Department, College of Engineering, AL-Mustaqbal University, 51001, Babylon, Iraq*

[d] *Department of Mechanical Engineering, Graphic Era (Deemed to be University), Dehradun 248002, Uttarakhand, India*

Abstract

In this work, rectangular plate samples are designed and fabricated using four arrangements: pure epoxy with a stiffener, pure epoxy plate without a stiffener, homogeneous composite plate with 0.5% V_f and a stiffener, and homogeneous composite plate with a FGM stiffener. The mathematical model is formulated based on the first-order shear deformation theory (FSDT). The free vibration test is conducted, and the signal is analyzed to obtain the free vibration characteristics. The results show that the homogeneous composite plate with 2% V_f and FGM stiffener exhibited a significant improvement in the natural frequency. However, using a Functionally Graded Material (FGM) stiffener and increasing the nano-volume fraction increases the natural frequency. Also, the plate without any filler (pure epoxy) and without a stiffener has the lowest frequencies among the composite plates employed. The discrepancy between the analytical and experimental techniques was no more than 10%.

Keywords: Composite plate; Stiffeners; Experimental work; Nano particles, Free Vibration

1. Introduction

Since recent advances in materials engineering and technology, significant progress has also been made, particularly owing to the emergence of composite materials. Such "designer" materials are currently very exciting; however, due to the new and tailorable properties exhibited by them that differ from those of traditional design-based materials. Moreover, functionally graded materials (FGMs) are an advanced type of composite material in which the property distribution varies through a specified direction. It varies softly and continuously with the gradient, i.e., very soft and special. In fact, FGMs are believed to possess a locally controllable continuous variation in the mechanical properties along the shaft length. FGMs are a new material in engineering and science fields, it had already offered various solutions through a multi-disciplinary spectrum of fields. Sandwich composite structures (SCS) are integral to the manufacturing of composite products and are utilized across a wide range of applications [1-4]. Recent technological advances have led to research on composite materials that are lighter, stronger, and more rigid. A stiffened nanostructure is a structural composite that integrates various elements to enhance overall

* Corresponding author. *E-mail address:* emad.njim@gmail.com

performance. Al-Shablle et al. [5] conducted free vibration analysis of a composite face sandwich plate reinforced with Al_2O_3 and SiO_2 nanoparticles.

Guo and Zhou [6] examined the free vibration of multiphase reinforced-resin-matrix composite shells with arbitrary boundaries and openings using a back-propagation neural network. Gao et al. [7] developed a micro-nanostructured green polyvinyl alcohol-based composite aerogel with enhanced mechanical properties, thermal insulation, and fire safety. Wang et al. [8] examined the nanoscale structure and sensitivity of self-sensing geopolymer composites reinforced with nanocarbon black. Zhang et al. [9] developed a TiC-$TiAl_3$ nano-interlayer and evaluated its impact on the thermo-physical properties of diamond/Al composites. Shishehsaz. M. et al. [10] performed finite element analysis of laminated composite plates using higher-order shear deformation theory to assess stress distribution in a five-layer sandwich plate, assuming continuous displacement across layers. They applied this analysis to a square, simply supported sandwich plate using layerwise theory. Nekoufar and Farrokhi [11] conducted a 3D free vibration analysis of carbon nanotube-reinforced FGM using the DQ method. Their findings include relationships for increasing the natural frequency, the lowest natural frequency, and the effects of the length-to-thickness ratio and changes in the dimensionless natural frequency in the beam.

Recent studies have examined the static and dynamic analysis on FG beam, plates and shells using various techniques [12-16]. Free vibration analysis is essential for assessing the dynamic performance of structural components under mechanical loading. This analysis determines natural frequencies, mode shapes, and damping characteristics essential for effective design. Shan et al. [17] reviewed how nano-additives affect the mechanical, impact, vibration, and buckling properties of composites. Zhang et al. [18] developed an analytical solution for magnetically tunable free-damped vibration in L-shaped composite spherical panels made of GPL-reinforced magneto rheological elastomers, using an element-based approach.

Neamah et al. [19] conducted a free-vibration analysis of intact and cracked laminated composite beams subjected to dynamic loading, using both experimental and finite-element methods. The study examined how crack properties affect the plate's natural frequency. Yu et al. [20] used a modified strain-gradient theory to investigated the mechanical stability of nano- polyethylene composites. They found that the nano size significantly improves the plate performance**.** Liu et al. [21] analyzed how nano-silica affects the material properties, pore structure, and hydration of polyacrylate/cement composites. They applied constitutive damage models to simulate the strength of composite sandwiches containing nano-silica particles at various temperatures and strain rates, thereby improving the accuracy of silica behavior predictions in complex loading scenarios. Experimental methods to evaluate how impactor shape influences the behavior of composite sandwich plates with an aluminium foam core under low-speed impact. By employing multiple types of impact cones, parabolic and spherical, a compressive and dynamic loading was used, providing insights into foam response under dynamic loading conditions. The mechanical properties of sandwiched constructions with composite and hybrid core structures, using open- and closed-loop designs, are investigated for flexural structural analysis [22].

Liu et al. [23] enhanced thermal performance, frost resistance, and pore structure in cement-based composites by introducing binary modifications with mPCMs/nano–SiO2. Using melt-spray technology, Liu et al. [24] fabricated composite microspheres doped with nanoaluminum powder. Sobhani investigated the free vibration problem in porous graphene oxide powder nanocomposites assembled in paraboloidal-cylindrical shells. Madan et al. [25] developed a two-step finite element method to estimate the thermo-mechanical properties of two-phase and three-phase hybrid composite materials. Sobhani and Masoodi [26] introduced a comprehensive shell approach for analyzing the vibration of porous nano-enriched polymer composites coupled with spheroidal-cylindrical shells. Abbas et al. [27] examined the mechanical properties of composite materials with various reinforcement types through both experimental and theoretical methods. Shi et al. [28] described the characterization and performance of a sol-gel composite zinc phosphate with a nanosheet structure, synthesized by modifying the sol-gel with silane.
Jankowski and Zur [29] examined steady-state vibration in nanocomposite structures with discontinuities. Saiah et al. [30] investigated the free vibration behavior of graphene-reinforced composite plies in laminated nanocomposites. Barcciocchi and Tarantino analyzed vibration and buckling in laminated composite nanoplates using strain gradients and third-order theory. Abbood et al. [31] studied the quasi-static and low-velocity impact behavior of laminated CFRP composites. Sobhani [32] explored the free vibration of porous graphene oxide powder nanocomposites assembled with paraboloidal-cylindrical shells.

M. Chwał [33] studied the Free Vibrations and Flutter Analysis of Composite Plates Reinforced with Carbon Nanotubes, While Hoang et al. [34] presented the free vibration analysis of a nanocomposite plate in contact with fluid using a novel quasi-3D shear deformation theory and an artificial neural network.

According to [35], Fabrication of microcrystalline cellulose and nano-titanium dioxide composites with broad-spectrum UV protection. Shan et al. [17] presented a review on the effects of nano-additives on the mechanical, impact, vibration, and buckling/post-buckling properties of composites. Many researchers conducted an experimental study on composite materials. For example, the effect of a hole notched in the fracture mechanics of

GLARE and GFRP composites subjected to quasi-static loading is investigated by [36]. Also, the experimental and analytical investigations of the forced and free vibrations of sandwich structures with reinforced composite faces in an acidic environment are presented in [37]. They examined the sensitivity of composite sandwich structures with different plate materials through both experimental and FEM analyses. Their results indicated that the contact force of a sandwich structure with a wood core exceeds that of a structure with a foam core. Damage was observed to initiate on the surfaces of both sandwich structures, subsequently progressing to plastic deformation and internal core damage. Ultimately, the rear surface composite panel also sustained damage.

Nosrati et al. [38] conducted a free vibration analysis of butterfly-shaped auxetic doubly curved nano-shells using the nonlocal strain gradient theory. Alireza Noruzi et al. [39] conducted a theoretical evaluation of a five-layer sandwich nanocomposite beam reinforced with graphene platelets (GPLs) and shape memory alloys (SMAs) to predict its deflection, buckling, and vibration under high dynamic loading. Hybrid joints with honeycomb cores are designed and developed. An analysis of the free vibration behavior of sandwich structures with honeycomb cores is conducted to determine their failure loads. Using the commercial FE software Abaqus, three joining strategies are numerically investigated and validated against experimental results.

The free vibration analysis of SPC-reinforced foam cores adopting micro-aluminum powder was explored using experimental and analytical techniques [40]. Khalvandi et al. [41] used an integration of supervised learning and experimentation to investigate the static and dynamic behavior of Y-shaped sandwich beams subjected to compressive loading. Finally, Singh and Jaiswal [42] analyzed the transverse vibration of piezo-electro-magneto-thermoelastic composite nanobeams under distinct Green–Naghdi III phase-lag models.

Stiffeners distribute loads more effectively and reduce the risk of deformation or failure under stress. Non-stiffened nanocomposite materials, by contrast, offer lighter weight, improved damping, and greater design flexibility due to their inherent properties. The selection between stiffened and non-stiffened nanocomposites depends on structural requirements, weight, and performance needs. Stiffeners are typically used in aircraft wings, fuselage, and tail sections, including vertical and horizontal stabilizers.

The existing literature reveals a scarcity of studies on the free vibration analysis of plates with hybrid composite stiffeners and functionally graded material (FGM) layers. However, this study aims to design and conduct free-vibration characterizations of rectangular composite plates using pure epoxy plates without stiffeners, pure epoxy plates with stiffeners, homogeneous composite plates with Silica nanoparticles and stiffeners, and homogeneous composite plates with FGM stiffeners and Nano Silica. The study is planned to fabricate composite plates using different techniques and derive the natural frequency equation analytically. The impact of various parameters, including volume fraction, stiffener materials, and geometrical properties, is considered.

2. Analytical model

Consider a stiffened rectangular plate with dimensions (*a, b*, and *h*) and the stiffeners are placed along one or both directions of the plate as illustrated in Figure 1.

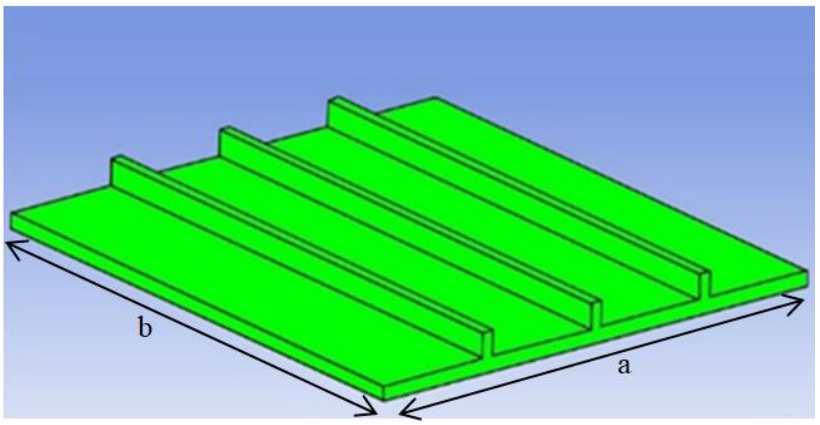

Fig. 1. The model of the stiffened composite rectangular plate structure

An FSDT states that the normal to the transverse direction does not remain perpendicular to the mid-surface after the deformation. It is assumed that the global displacement field, denoted by left. $(\mathbf{u}^{\sim}, \mathbf{v}^{\sim}, \mathbf{w}^{\sim})$, at any random position within the panel is:

$$\tilde{u}(x,y,z,t) = u(x,y,t) + z\phi_x(x,y,t)$$
$$\tilde{v}(x,y,z,t) = v(x,y,t) + z\phi_y(x,y,t) \quad (1)$$
$$\tilde{w}(x.y.z.t) = w(x.y.t)$$

where $(\boldsymbol{\phi_x}, \boldsymbol{\phi_y})$ illustrate the transverse normal of the slopes around $(\mathbf{y})$ and $(\mathbf{x})$ axes at $(\mathbf{z} = \mathbf{0})$. The stress-strain relation for a plate and the nonlinear Von Karman terms are given by:

$$\begin{pmatrix}\varepsilon_x\\ \varepsilon_y\\ \gamma_{xy}\end{pmatrix} = \begin{pmatrix}\varepsilon_x^\circ\\ \varepsilon_y^\circ\\ \gamma_{xy}^\circ\end{pmatrix} + z\begin{pmatrix}\lambda_x\\ \lambda_y\\ \lambda_{xy}\end{pmatrix}. \quad \begin{pmatrix}\gamma_{xz}\\ \gamma_{yz}\end{pmatrix} = \begin{pmatrix}\frac{\partial w}{\partial x} + \phi_x\\ \frac{\partial w}{\partial y} + \phi_y\end{pmatrix}. \begin{pmatrix}\varepsilon_x^\circ\\ \varepsilon_y^\circ\\ \gamma_{xy}^\circ\end{pmatrix} = \begin{pmatrix}\frac{\partial u}{\partial x} + \frac{1}{2}\left(\frac{\partial w}{\partial x}\right)^2\\ \frac{\partial v}{\partial y} + \frac{1}{2}\left(\frac{\partial w}{\partial x}\right)^2\\ \frac{\partial u}{\partial y} + \frac{\partial v}{\partial x} + \frac{\partial w}{\partial x}\frac{\partial w}{\partial y}\end{pmatrix}.$$

$$\begin{pmatrix}\lambda_x\\ \lambda_y\\ \lambda_{xy}\end{pmatrix} = \begin{pmatrix}\frac{\partial \phi_x}{\partial x}\\ \frac{\partial \phi_y}{\partial y}\\ \frac{\partial \phi_x}{\partial y} + \frac{\partial \phi_y}{\partial x}\end{pmatrix} \quad (2)$$

where $(\gamma_{xz}, \gamma_{yz})$ illustrate the components of transverse shear strains in the planes. (xz, yz). Based on Hooke's law, the nonlinear strain-stress relations for a plate may be stated as follows.

$$\begin{bmatrix}\sigma_x\\ \sigma_y\\ \tau_{xy}\\ \tau_{yz}\\ \tau_{xz}\end{bmatrix} = \begin{pmatrix}C_{11} & C_{12} & 0 & 0 & 0\\ C_{12} & C_{22} & 0 & 0 & 0\\ 0 & 0 & C_{66} & 0 & 0\\ 0 & 0 & 0 & C_{44} & 0\\ 0 & 0 & 0 & 0 & C_{55}\end{pmatrix}\begin{bmatrix}\epsilon_x\\ \epsilon_y\\ \gamma_{xy}\\ \gamma_{yz}\\ \gamma_{xz}\end{bmatrix}, \quad C_{11}^{(j)} = C_{22}^{(j)} = \frac{E^{(j)}(z)}{1-\nu^2}, C_{12}^{(j)} = \frac{\nu E^{(j)}(z)}{1-\nu^2},$$
$$C_{44}^{(j)} = C_{55}^{(j)} = C_{66}^{(j)} = K_s\frac{E^{(j)}(z,T)}{2(1+\nu)} \quad (3)$$

Where (K_s) is the factor used to adjust for shear and is given by $\left(K_s = \frac{5}{6}\right)$.

The Governing equations:

$$\delta u: \frac{\partial N_x}{\partial x} + \frac{\partial N_{xy}}{\partial y} = I_0\frac{\partial^2 u}{\partial t^2} + I_1\frac{\partial^2 \phi_x}{\partial t^2}, \delta v: \frac{\partial N_{xy}}{\partial x} + \frac{\partial N_y}{\partial y}$$
$$= I_0\frac{\partial^2 v}{\partial t^2} + I_1\frac{\partial^2 \phi_y}{\partial t^2}, \delta w: \frac{\partial Q_x}{\partial x} + \frac{\partial Q_y}{\partial y} + N_x\frac{\partial^2 w}{\partial x^2} + 2N_{xy}\frac{\partial^2 w}{\partial x\,\partial y} + N_y\frac{\partial^2 w}{\partial y^2} + q = I_0\frac{\partial^2 w}{\partial t^2}$$
$$\delta Q_x: \frac{\partial M_x}{\partial x} + \frac{\partial M_{xy}}{\partial y} - Q_x = I_2\frac{\partial^2 \phi_x}{\partial t^2} + I_1\frac{\partial^2 u}{\partial t^2}, \delta Q_y: \frac{\partial M_{xy}}{\partial x} + \frac{\partial M_y}{\partial y} - Q_y = I_2\frac{\partial^2 \phi_y}{\partial t^2} + I_1\frac{\partial^2 v}{\partial t^2} \quad (4)$$

where,

$$N_x = \int_{-\frac{h}{2}}^{\frac{h}{2}}\sigma_x\,dz + \Phi_1, N_y = \int_{-\frac{h}{2}}^{\frac{h}{2}}\sigma_y\,dz + \Phi_1, N_{xy} = \int_{-\frac{h}{2}}^{\frac{h}{2}}\sigma_{xy}dz, M_x = \int_{-\frac{h}{2}}^{\frac{h}{2}}\sigma_x\,z dz + \Phi_2,\ M_y = \int_{-\frac{h}{2}}^{\frac{h}{2}}\sigma_y\,z dz + \Phi_2$$
$$M_{xy} = \int_{-\frac{h}{2}}^{\frac{h}{2}}\sigma_{xy}z\,dz$$
$$(Q_x, Q_y) = \int_{-\frac{h}{2}}^{\frac{h}{2}}(\sigma_{xz}, \sigma_{yz})\,dz, \Phi_1 = -\frac{1}{1-\upsilon}\int_{-\frac{h}{2}}^{\frac{h}{2}}E(z)\,dz\,), \quad \Phi_2 = -\frac{1}{1-\upsilon}\int_{-\frac{h}{2}}^{\frac{h}{2}}E(z,T)\,.\,dz \quad (5)$$

The symbols can denote the force resultants of a plate (N_x, N_y, N_{xy}), while the moment resultants can be represented by the symbols (M_x, M_y, M_{xy}), and the transverse force resultants can be denoted by (Q_x, Q_y).

When Equation (7) is placed into Equation (10) taking Equation (6) into consideration, the following results are obtained:

$$N_x = I_{10}\varepsilon_x^\circ + I_{20}\varepsilon_y^\circ + I_{11}\frac{\partial \phi_x}{\partial x} + I_{21}\frac{\partial \phi_y}{\partial y} + \Phi_1,\quad N_y = I_{20}\varepsilon_x^\circ + I_{10}\varepsilon_y^\circ + I_{21}\frac{\partial \phi_x}{\partial x} + I_{11}\frac{\partial \phi_y}{\partial y} + \Phi_1,$$

$$N_{xy} = I_{30}\gamma_{xy}^\circ + 2I_{31}\left(\frac{\partial \phi_x}{\partial y} + \frac{\partial \phi_y}{\partial x}\right), \tag{6a}$$

$$M_x = I_{11}\varepsilon_x^\circ + I_{21}\varepsilon_y^\circ + I_{12}\frac{\partial \phi_x}{\partial x} + I_{22}\frac{\partial \phi_y}{\partial y} + \Phi_2,\ M_y = I_{21}\varepsilon_x^\circ + I_{11}\varepsilon_y^\circ + I_{22}\frac{\partial \phi_x}{\partial x} + I_{12}\frac{\partial \phi_y}{\partial y} + \Phi_2,\ M_{xy}$$

$$= I_{31}\gamma_{xy}^\circ + I_{32}\left(\frac{\partial \phi_x}{\partial y} + \frac{\partial \phi_y}{\partial x}\right), Q_x = K_s I_{30}\gamma_{xz}, Q_y = K_s I_{30}\gamma_{yz},$$

$$w = N_{xy} = \phi_y = 0, N_x = N_{x0}, \qquad \text{at } x = 0, a,$$

$$w = N_{xy} = \phi_x = 0, N_y = N_{y0}, \qquad \text{at } y = 0, b, \tag{6b}$$

- **Analytical solution for composite plate with nanoparticles**

The mathematical modeling of free vibrations in a stiffened rectangular plate with nanoparticles involves several considerations to represent the behavior of the structure. With the presence of the nanoparticles, the effective material properties formoulation includes modulus of elasticity (E), Possions ratio (ν) and mass density are;

$$E_{eff} = E_{matrix}(1-\psi) + E_{np}\psi \tag{7a}$$

$$\rho_{eff} = \rho_{matrix}(1-\psi) + \rho_{np}\psi \tag{7b}$$

where ψ is the volume fraction of the nanoparticles, E_{matrix}, ρ_{matrix}, E_{np}, ρ_{np} are the young modulus and density oft he matrix material and nanoparticles respectively.

The equations of motion for the free vibration of a stiffened composite plate can be generated using the principle of virtual work or Lagrange's equations.

.

$$D\nabla^4\,\omega(x,y) + M\frac{\partial^2 \omega(x,y)}{\partial t^2} \tag{8a}$$

$$D = \frac{E_{eff}h^3}{12(1-\nu)} \tag{8b}$$

M: is the mass per unit area, M= $\boldsymbol{\rho_{eff}}$ h.

The mode shape is stated as follows because it has to meet the constraints that are provided in Equation (8):

$$w(x.y.t) = W(t)\sin\lambda_m x \sin\delta_n y.\ \phi_x(x.y.t) = \Phi_x(t)\cos\lambda_m x \sin\delta_n y.\ \phi_y(x.y.t)$$

$$= \Phi_y(t)\sin\lambda_m x \cos\delta_n y \tag{9}$$

Plug (9) into (10) to get the stress function coefficients:

$$\begin{pmatrix} A_{11}\frac{\partial^4 f}{\partial x^4} + A_{22}\frac{\partial^4 f}{\partial y^4} + (A_{66} - 2A_{12})\frac{\partial^4 f}{\partial x^2 \partial y^2} - B_{21}\frac{\partial^3 \phi_x}{\partial x^3} - B_{12}\frac{\partial^3 \phi_y}{\partial y^3} \\ +(B_{66} - B_{11})\frac{\partial^3 \phi_x}{\partial x \partial y^2} + (B_{66} - B_{22})\frac{\partial^3 \phi_y}{\partial x^2 \partial y} - \left(\frac{\partial^2 w^2}{\partial x \partial y} - \frac{\partial^2 w}{\partial x^2}\frac{\partial^2 w}{\partial y^2}\right) \end{pmatrix} = 0 \tag{10}$$

$$\tilde{f}(x,y,t) = \begin{pmatrix} \tilde{A}_1(t)\cos 2\lambda_m x + \tilde{A}_2(t)\cos 2\delta_n y + \\ \tilde{A}_3(t)\sin\lambda_m x \sin\delta_n y + \frac{1}{2}N_{x0}y^2 + \frac{1}{2}N_{y0}x^2 \end{pmatrix} \tag{11}$$

where,

$$\widetilde{A}_1(t) = \frac{\delta_n^2}{32A_{11}\lambda_m^2}W^2, \delta_1 = (-1)^m - 1, \delta_2 = (-1)^n - 1$$

$$\lambda = \frac{a}{b}, \widetilde{A}_2(t) = \frac{\lambda_m^2}{32A_{22}\delta_n^2}W^2, \widetilde{A}_3(t) = \frac{[B_{21}\lambda_m^3 + (B_{11} - B_{66})\lambda_m\delta_n^2]\Phi_x(t) + [\delta_n^3 B_{12} + (B_{22} - B_{66})\lambda_m^2\delta_n]\Phi_y(t)}{[A_{11}\lambda_m^4 + A_{22}\delta_n^4 + (A_{66} - 2A_{12})\lambda_m^2\delta_n^2]}, \quad (12)$$

Consider the finite-geometry model of a thin plate with four corners that are simply supported and immobile, expose d to thermal stresses. The circumstances shown by the immovable on the margins are as follows:
$u = 0$ on $x = 0, a$ and $v = 0$ on $y = 0, b$,

$$\int_0^a \int_0^b \frac{\partial u}{\partial x} dxdy = 0, \int_0^a \int_0^b \frac{\partial v}{\partial y} dxdy = 0 \quad (13)$$

$$\frac{\partial u}{\partial x} = A_{22}\frac{\partial^2 f}{\partial y^2} - A_{12}\frac{\partial^2 f}{\partial x^2} - B_{11}\frac{\partial \phi_x}{\partial x} - B_{12}\frac{\partial \phi_y}{\partial y} - \frac{1}{2}\left(\frac{\partial w}{\partial x}\right)^2 + C_{11}^*\Phi_1 + \Phi_2, \frac{\partial v}{\partial y} = A_{11}\frac{\partial^2 f}{\partial x^2} - A_{12}\frac{\partial^2 f}{\partial y^2} - B_{21}\frac{\partial \phi_x}{\partial x} -$$

$$B_{22}\frac{\partial \phi_y}{\partial y} - \frac{1}{2}\left(\frac{\partial w}{\partial y}\right)^2 + C_{22}^*\Phi_1 + \Phi_2 \quad (14)$$

The free vibration problem for the plate can be solved using

$$(K - \omega^2{}_n M)\omega^*{}_n = 0 \quad (15)$$

3. Experimental work

Experiments and discussion. The experimental section is divided into 2 stages: a) -The experiment. Production In the initial phase of the study, structures made of stiffened nanocomposite plates, with a polymer mould as the matrix reinforced by silica nanofillers, are investigated and compared with the corresponding stiffened and unstiffened pure plates, along with an FGM grey-colored AM gate. The second stage is subjected to a machine-sample vibration test, which was carried out using a dynamic loading method to determine the basic natural frequency and damping ratio of the structure.

For this study, Epoxy resin was Sikadur®-52 LPEpoxide of Bisphenol A (epichlorhydrin), Oxiran mono (C-12-14 alkyloxy) methyl derivatives. It is a two-part solvent-free, low-viscosity injection liquid based on high-strength epoxy resins. Also, important material variables of the Epoxy Resin include its tensile strength (~27.5 MPa) and Poisson's Ratio (0.34). The hardener was 3-aminomethyl-3,5,5-trimethyleyclohexylamine3,6-dizaoctaneethylene diamine.

In the present study, the nanoparticle reinforcements were silica which was procured from Guangzhou Billion Peak Chemical-Technology Co., Ltd. Their primary physical attributes are: (average particle size 14-36 nm), specific surface area (585 ± 25 m^2/g, purity (99.89 %) and mechanical parameters such as Young's Modulus = 70.5 GPa and Poisson =0.185).

- **Dies Preparation**

Two acrylic molds (6 mm thick) were used to make the samples. The molds were designed in SolidWorks software and machined on a computer numerical controlled (CNC) machine, followed by two-level polishing in the first stage to remove defects from the faces without cracks, as shown in the figure. 2. gradation We prepared emery papers (400) and (1000) for this purpose.

The first mold consists of two layers. The lower layer is used as a base to prevent mixture leakage with dimensions of (36*36*0.6) cm^r, and the middle layer contains grooves of the sample shape required forms with outer dimensions of (36*36*0.6) cm^3 and inner dimensions of (26*26*0.6) cm^3. This mold used to produce unstiffened plates.

The second mold consists of three layers. The lower layer is used as the base, and the middle layer contains grooves of the sample shape required forms with the same dimension of the first mold and the upper layer is square dimensions of (26*26*0.6) cm^3, which contains three stiffeners with dimensions (0.6*1*26) cm^3. This mold used to produce plates with three stiffeners. Before the pouring process inside the mold, the molds are securely assembled using screws through the holes made in all layers, to prevent material leakage during pouring. as shown in Figure 3.

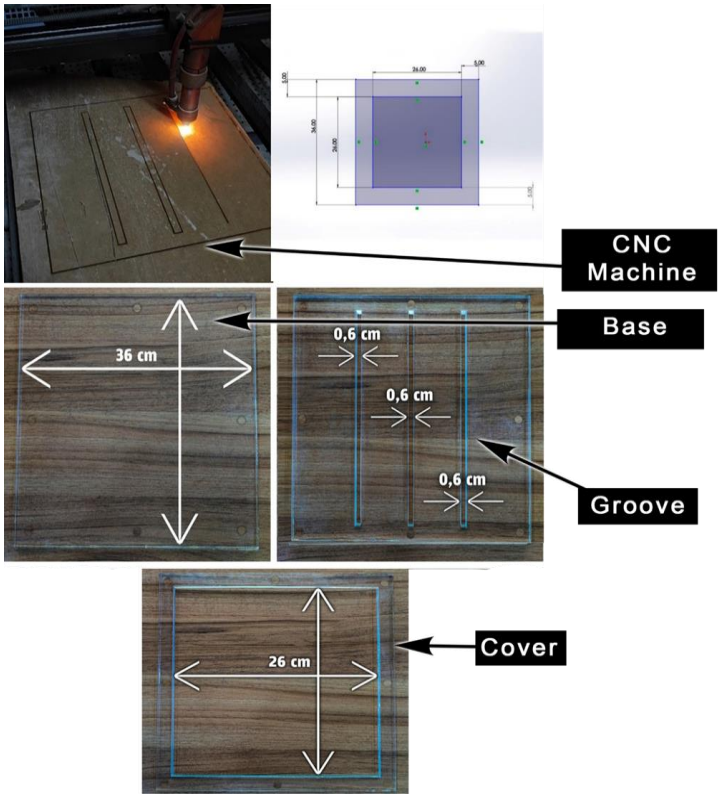

Fig. 2. Design an Acrylic mold for fabricating homogenous composite samples

Fig. 3. Fabricated Acrylic mold different sample arrangement used in this study

- **Calculation Density of nano particles:**

Density measurements were performed by calculating the nanoparticles' density as the ratio of their mass to volume, using a cylindrical beaker containing a solvent (thinner). This process resulted in obtaining the density of SiO_2, which equals 2.37 g/cm³ as shown in Figure 4.

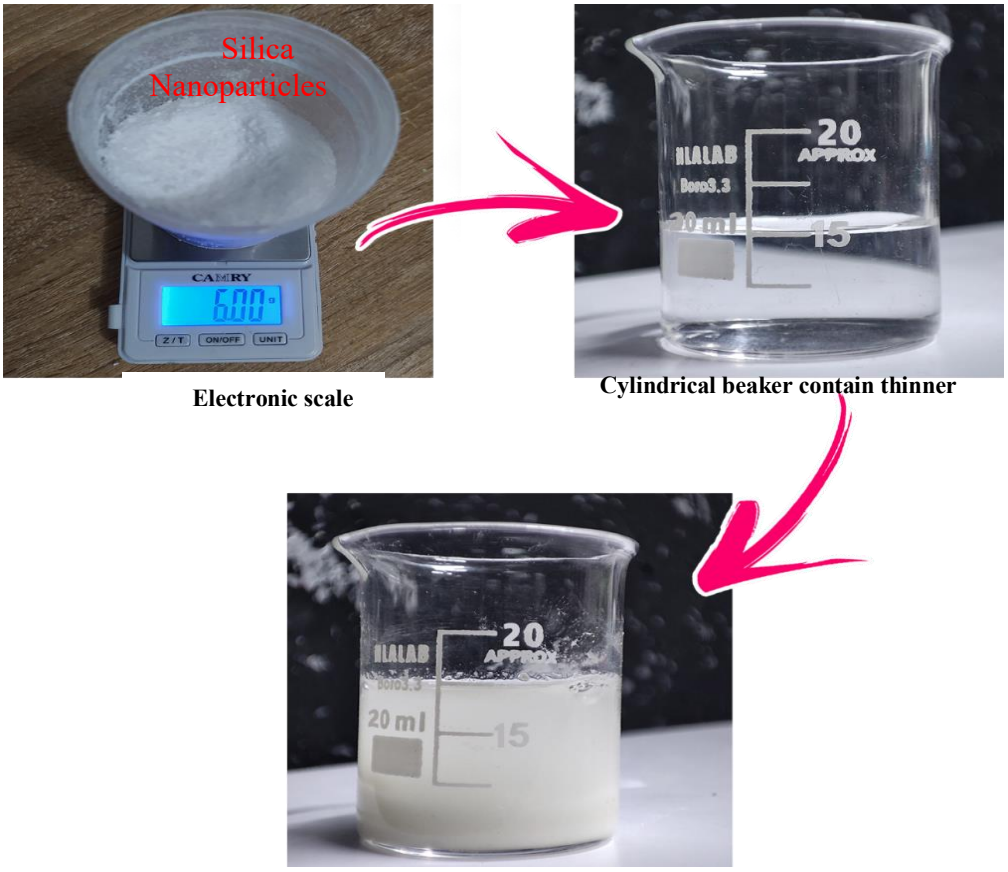

Electronic scale **Cylindrical beaker contain thinner**

Fig 4. Measuring the density of nanoparticles.

- **Nanocomposites Preparation**

Those nanocomposites were developed using hand lay-up. Having homogenized the paste, it is mixed with a resin in an appropriate solution (diluent), to which all reinforcement has been previously added. To bring other models (made of neat epoxy) successively to those conditions established in this way, for each resin, an amount of volume of the thinner solvent (ethylene glycol butyl ether) was placed. The mixture was stirred for 15 min after standing for 30 min, then placed in a vacuum chamber. One of those is an oven which has to dry the paint to its max - under vacuum (with vac. pump). After the hardener was sucked to dryness, the stoichiometric ratio of the hardener 4 (epoxy)/1 (hardener) was stirred for 15 min in a homogeneous mixture, and was bubble-free by using a vacuum pump in 5 min. The mixture was then poured into a room-temperature acrylic mold and allowed to cure for 2 days.

For the preparation of isotropic epoxy/nanoparticles, different weight % (0.5,1.5, and 2) % V_f SiO_2 reinforcement are dissolved in a sufficient quantity of the above-mentioned solution previously. Then the mixture was mixed well with the help of a magnetic stirrer and sonicated amplitude 75% for 15 min, with time intervals at 50s ON and 10s OFF. The proper amount of epoxy was added to the mixture in the manner described above. Its mechanical stirring was 15 min, and it was degassed at the vacuum pump over a period of 30 min to eliminate any build-up of air bubbles and evaporate its thinner.

The stoichiometric ratio of hardener added was 1:1, and the mixture was slowly hand-stirred for 30 min to degas using a vacuum pump, with air bubbles accompanying 5. Hereafter, the homogeneous slurry was cast into an acrylic mold and left to cure for 2 days. This phenomenon can also be observed in Fig. 5. The prepared samples are shown to be pure and homogeneous in Figures 6 and 7.

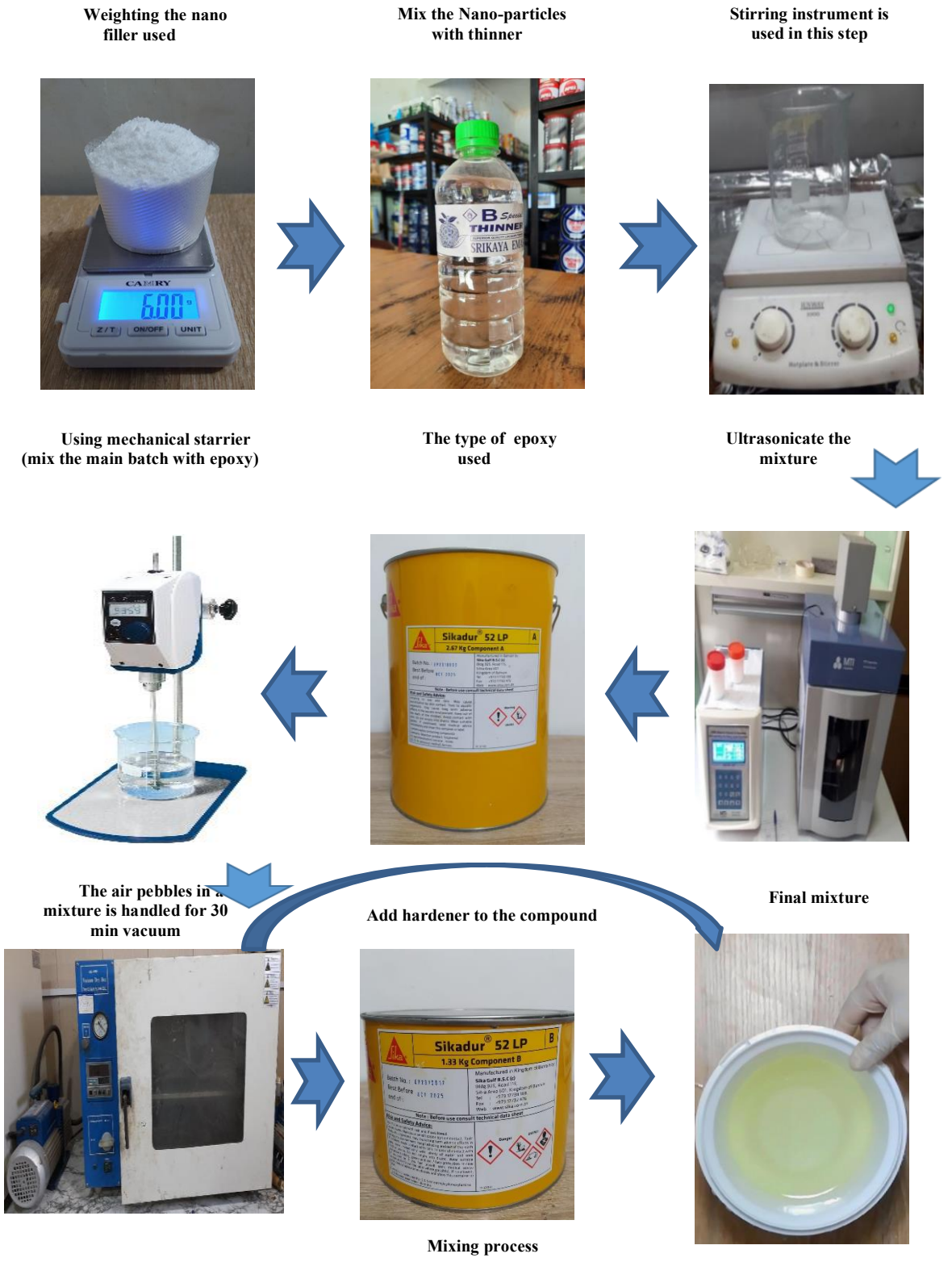

Fig. 5. The work plan used in fabricating FGNC.

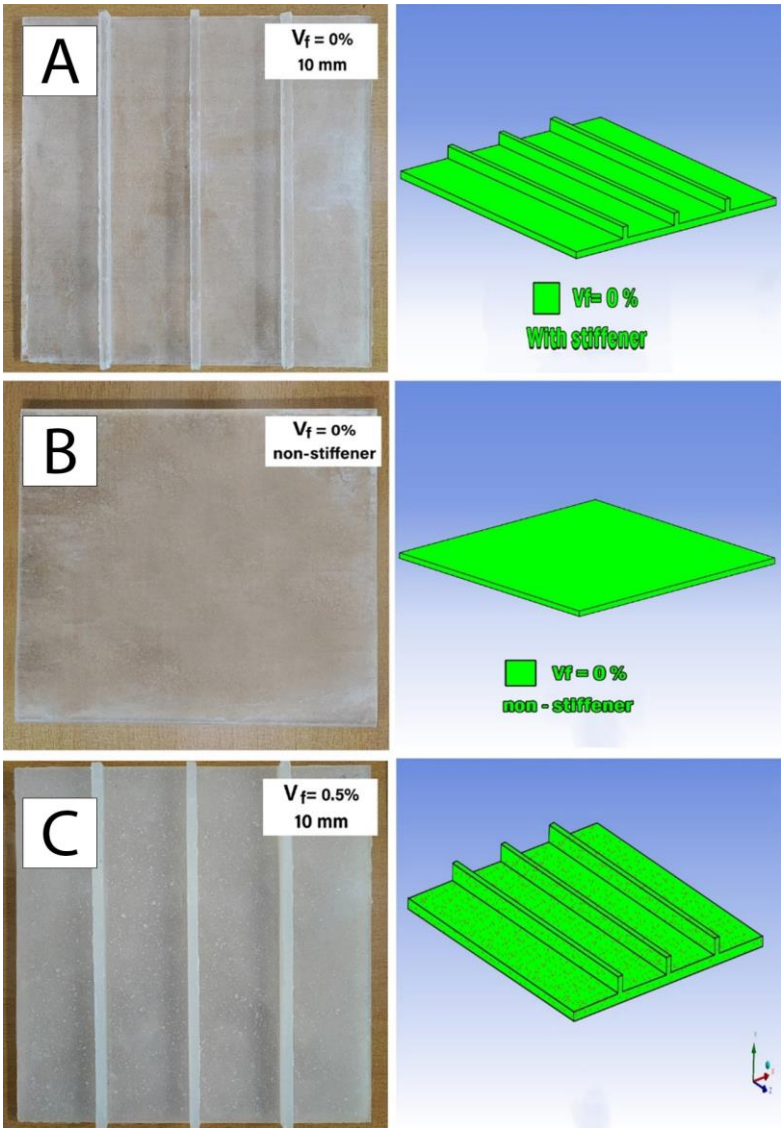

Fig 6. Show different types of samples (A): Pure epoxy with stiffeners (B): Pure epoxy without stiffeners (C): Homogenous composite plate o.5% V_f with stiffener.

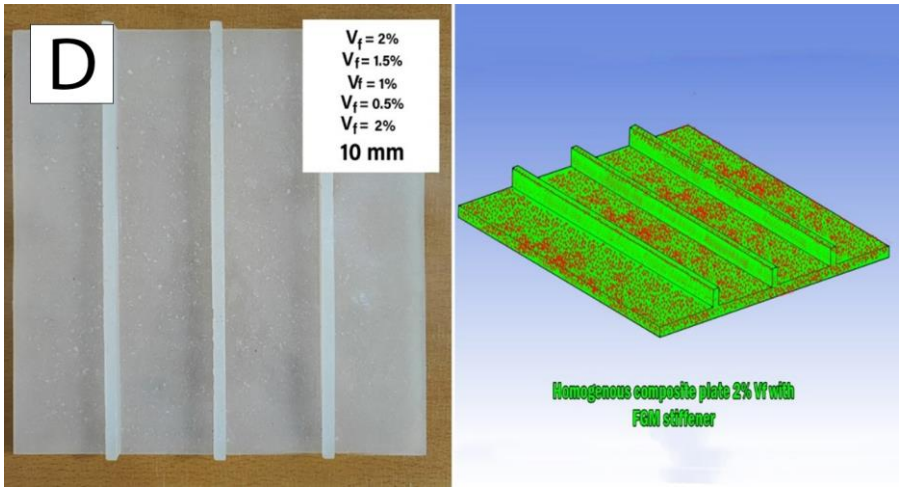

Fig 7. Show different types of samples (D): Homogenous composite plate 2% V_f with FGM stiffener

- **Preparation of FGPNC Stiffeners**

Figures 8 and 9 illustrate the functionally graded polymer nanocomposite (FGNC) stiffener plate. The fabrication process for the FGNCs involved two primary stages. First, the nanofiller and liquid matrix were combined using appropriate dispersion and mixing techniques, as previously described for the isotropic nanocomposite. Next, the liquid mixture was sequentially cast into layers within acrylic molds, following a predetermined graded structure. Each layer was fabricated with 2.5 mm thick.

Fabrication of the FGM stiffener began by pouring the required amount of neat epoxy into a mold to form a 2.5 mm-thick layer, which was cured for 1 hour. A nanocomposite layer containing 0.5% volume fraction (V_f) of silica nanoparticles was then cast onto the semi-cured epoxy and cured for an additional hour. Subsequently, three nanocomposite layers with 1%, 1.5%, and 2% V_f of silica nanoparticles, respectively, were sequentially cast and cured, resulting in a total stiffener thickness of 6 mm. This procedure was repeated for all FGM stiffener samples.

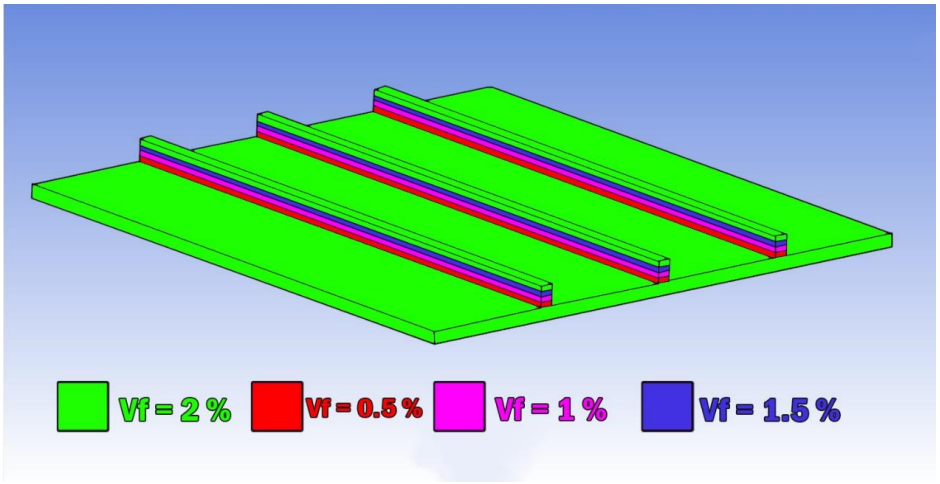

Fig 8. Sample of functionally graded silica nanocomposites (FGSNC) With different areas to measure hardness in the Solid Work program

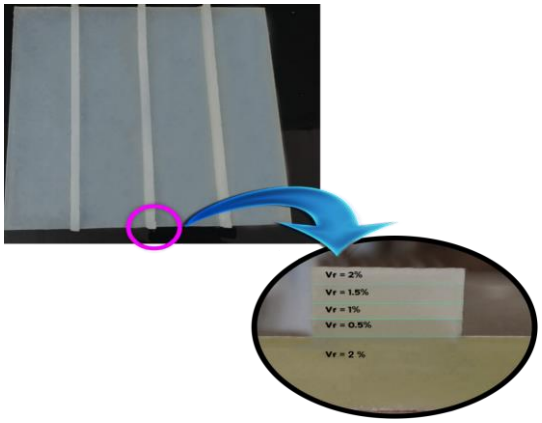

Fig 9. Sample of functionally graded silica nanocomposites (FGSNC) with different areas to measure hardness.

- **Vibration Test of Stiffened and Unstiffened Samples:**

The vibration tests utilize free and forced vibration behavior of plates. The free vibration tests are conducted to obtain the natural frequency of plates and mode shapes. The mode shapes are the shapes that the structure takes when vibrating at its natural frequency. There are multiple such frequencies, but a few of which are at the lowest frequency are important. Fig. 10 shows that the stiffened and unstiffened plates were manufactured with the specified dimensions. The stiffened rectangular specimen is made from 3-stiffeners with a clamped free boundary condition. The parts and machines that are used in the vibration test are shown in Figures 11 and 12.

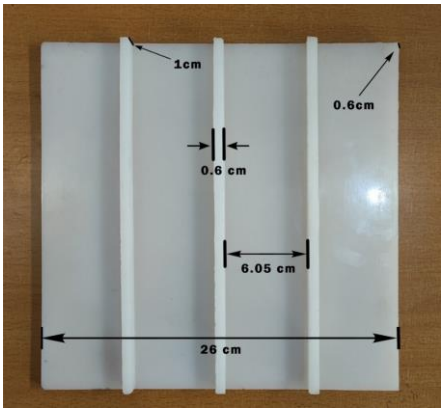

Fig. 10. The plate with stiffeners

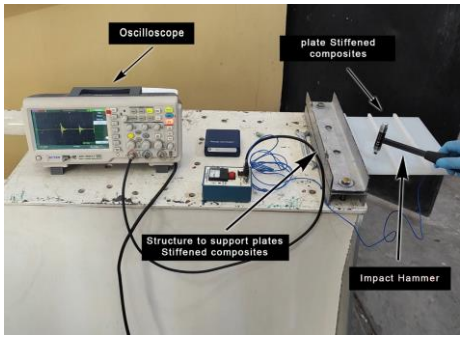

Fig. 11. Rig and Vibration Test Machine of Plates Stiffened Composites.

The vibration testing system comprises several reliable components. The primary support structure is a steel plate of specified thickness. An impact hammer (model 086C01, PCB Piezotronics Vibration Division) is employed to excite the sample. An accelerometer (model 353C68) is attached to the structure using a magnetic mount to record vibration signals. The accelerometer response is measured using an amplifier (model 480E09), which outputs the signal to a digital storage oscilloscope. This low-noise charge amplifier is designed for use with piezoelectric accelerometers and other piezoelectric transducers, providing wide-range signal conditioning by adjusting the voltage range. This feature makes it suitable for accelerometer calibration setups and general vibration measurements. The digital storage oscilloscope (model ADS 1202CL+) shown in Fig. 12 features a maximum sampling rate of 500 MSa/s, a maximum frequency of 200 MHz, and two input channels. The oscilloscope displays the accelerometer response waveform for the stiffened cylindrical shell. The response signal is acquired from the oscilloscope using the SigView program and processed with a fast Fourier transform (FFT) function to determine the fundamental natural frequency.

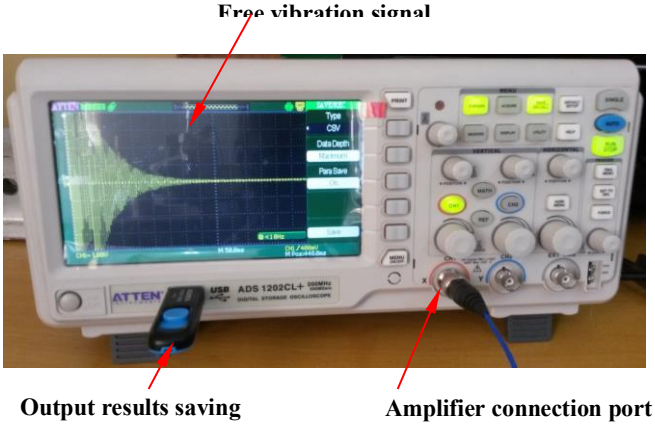

Fig. 12. The free vibration test measurement.

This study employs the roving accelerometer test. The stiffened cylindrical shell is struck once at the upper free edge, and a single accelerometer is positioned at five locations, as shown in Fig. 13. To determine the fundamental natural frequency and damping ratio, an impact hammer generates an impulse, and the accelerometer records the response at various points on the model. The signal can be measured in three ways.

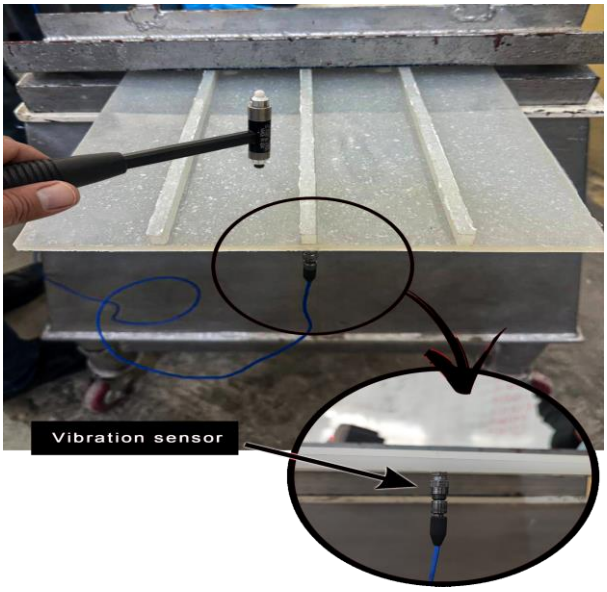

Fig. 13. Location of Accelerometer and Impact Hammer on the Plates Stiffened Composites.

Response and transient load signals are recorded by the digital storage oscilloscope as images and Excel files. These signals are then processed using the Sig-View program. The FFT function is applied to analyze the response of the tested stiffened cylindrical shell and determine the fundamental natural frequency, as shown in Fig. 13. The damping ratio was calculated from the response from digital oscilloscope by using curve fitting method using logarithmic increment method.

4. Results

Figures 14 to 21 show the frequency results of the four-configuration used in this study as obtained by FFT analysis. The numerical analysis results generally align with the analytical results, though minor discrepancies are present. These differences are due to material properties, analytical assumptions, and plate structure. Table 1 presents the results and discrepancies. It is found from the results that the addition of two layers with uniform separation, thickness and edge length has significantly pushed up the natural frequency of pure epoxy plane plate from ~34.34 Hz to 160.7 Hz, i.e., more than four times improvement in stiffness characteristics was attained. Additional enhancement to the pressure wave is achieved by reinforcement. When a 0.5% volume fraction with stiffener is considered frequency value is 161.39 Hz, which shows little deviation, but when compared to the stiffened pure epoxy, we can conclude that the addition of even a small amount of fiber will increase stiffness. Its maximum frequency with 2% fiber content and FGM stiffened comes close to 250 Hz. This extraordinary enhancement is due to the fiber reinforcement along with the graded stiffness in the FGM stiffener. Overall, the results show that material type and stiffener layout as critical design factors to dictate dynamic gains; FGMX-stiffened composite achieved the optimum performance. The discrepancy in the analytical and experimental results was below 11% indicates the proper fabrication of sandwich plates. However, in this work, it is shown that the benefit of using stiffeners in composite materials is improved structural integrity and stiffness, which enhances the overall strength-to-weight ratio of the component or structure.

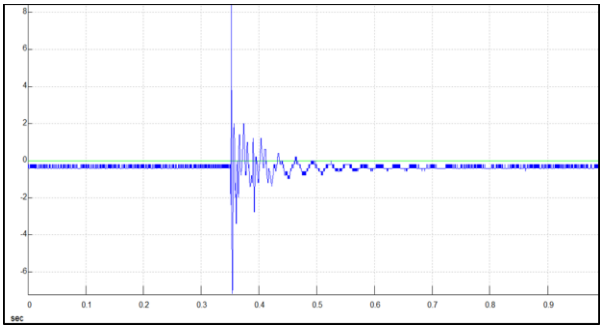

Fig. 14. Experimental response in time domain for pure epoxy without stiffeners.

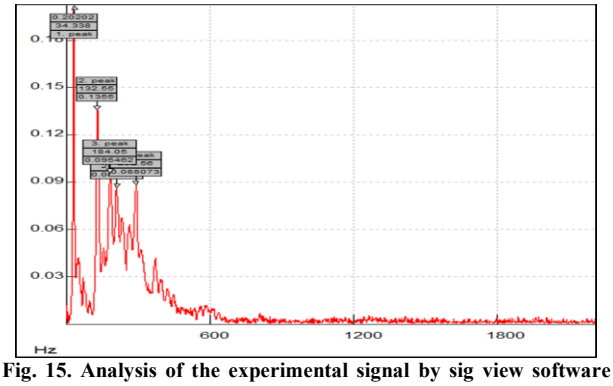

Fig. 15. Analysis of the experimental signal by sig view software for pure epoxy without stiffeners.

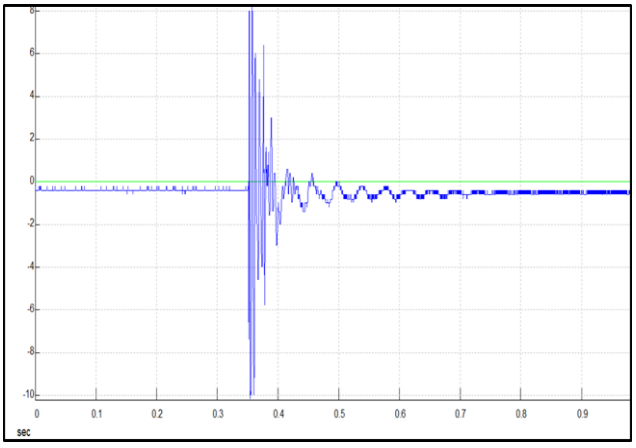

Fig. 16. Experimental response in time domain for pure epoxy with stiffeners.

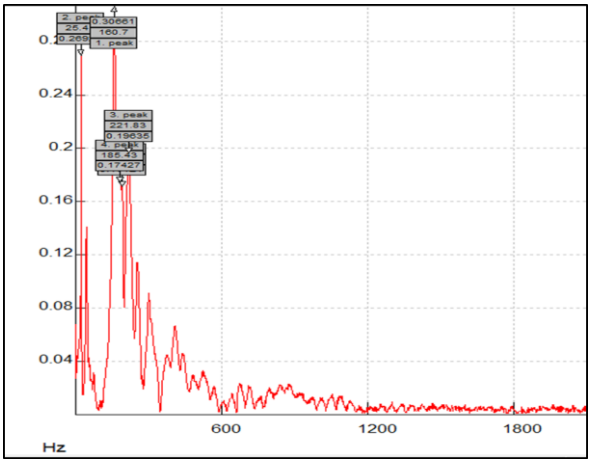

Fig. 17. Analysis of the experimental signal by sig view software for pure epoxy with stiffeners.

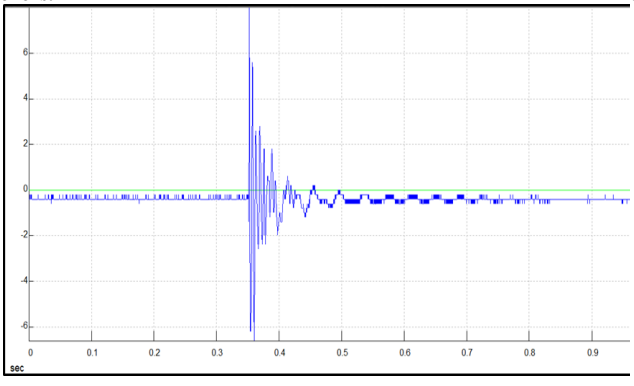

Fig. 18. Experimental response in time domain for 0.5% V_f SiO_2 nanocomposite without stiffeners.

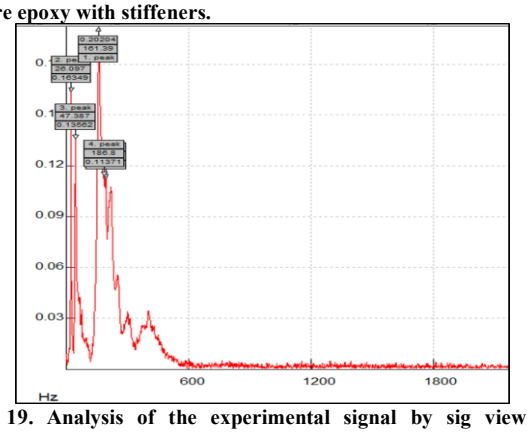

Fig. 19. Analysis of the experimental signal by sig view software for 0.5% V_f SiO_2 nanocomposite with stiffeners.

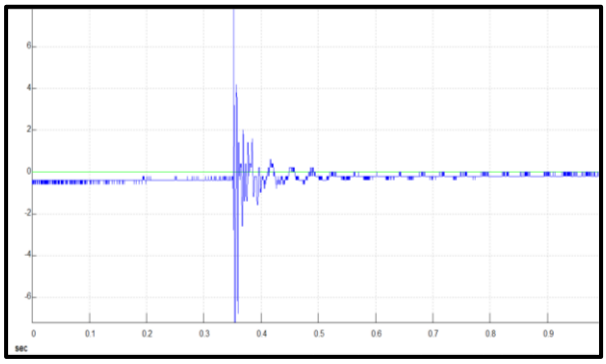

Fig. 20. Experimental response in time domain for homogenous nano-composite 2%vf with FGM stiffeners.

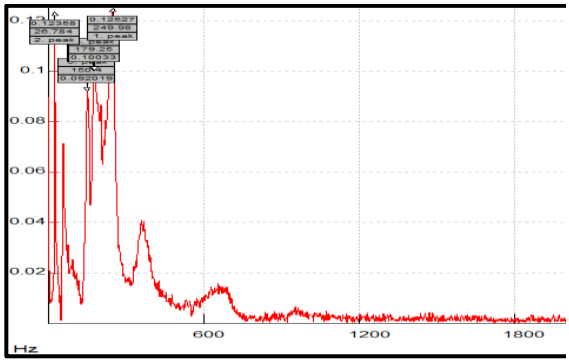

Fig. 21. Analysis of the experimental signal by sig view software for homogenous nano-composite 2%vf with FGM stiffener.

Table 1. Experimental and Numerical Fundamental Natural Frequency Results of different Plates

Sample Type	Analytical Frequency (Hz)	Analytical Frequency (Hz)	Discrepancy (%)
Pure epoxy plate without stiffener	34.338	36.75	6.56
Pure epoxy plate with stiffener	160.7	172.89	7
Homogenous composite plate 0.5% Vf with stiffener	161.39	179.00	9.8
Homogenous composite plate 2% Vf with FGM stiffener	249.98	268.56	7

5. Conclusions

This study investigates the free vibration behavior of stiffened composite plates using both analytical modeling and experimental methods. An estimation of mechanical properties and a determination of natural frequency were performed. In this study, four types of plate material arrangement are considered (Pure epoxy plates without stiffeners, Pure epoxy plates with stiffeners, Homogenous composite plates 0.5% V_f with stiffeners, and Homogenous composite plates 2% V_f with FGM stiffeners). A simulation of the experimental approach is conducted by analytical modeling, and the natural frequency results are compared. The results produced by this method are satisfactory. In summary, the following important observations can be recorded from this investigation.

1. Using an FGM instead of a traditional composite or stiffener reduces mass and cost while maintaining performance.
2. A homogeneous composite plate with a 2% volume fraction and an FGM stiffener significantly improves free vibration characteristics.
3. The pure epoxy plate without a stiffener exhibits the lowest natural frequency observed in this study.
4. For the homogeneous composite plate with a stiffener, the optimal volume fraction is 0.5.
5. The maximum discrepancy between experimental and analytical solutions does not exceed 10%.

Acknowledgements

The authors thank Najaf Technical Engineering College, Al-Furat Al-Awsat Technical University, Najaf, Iraq, for providing the facilities for this work.

References

[1] D. Van Doan, P. Van Minh, T. Van Ke, N. T. C. Nhung, D. Van Thom, An Overview of Functionally Graded Materials: From Civil Applications to Defense and Aerospace Industries, *Journal of Vibration Engineering & Technologies,* Vol. 13, No. 1, pp. 68, 2025/01/10, 2025.

[2] S. Alkunte, I. Fidan, V. Naikwadi, S. Gudavasov, M. A. Ali, M. Mahmudov, S. Hasanov, M. Cheepu, Advancements and Challenges in Additively Manufactured Functionally Graded Materials: A Comprehensive Review, *Journal of Manufacturing and Materials Processing,* Vol. 8, No. 1, pp. 23, 2024.

[3] S. Yadav, S. Liu, R. K. Singh, A. K. Sharma, P. Rawat, A state-of-art review on functionally graded materials (FGMs) manufactured by 3D printing techniques: Advantages, existing challenges, and future scope, *Journal of Manufacturing Processes,* Vol. 131, pp. 2051-2072, 2024/12/12/, 2024.

[4] T. Nakamura, T. Wang, S. Sampath, Determination of properties of graded materials by inverse analysis and instrumented indentation, *Acta Materialia,* Vol. 48, No. 17, pp. 4293-4306, 2000/11/08/, 2000.

[5] M. Al-Shablle, E. K. Njim, M. J. Jweeg, M. Al-Waily, Free vibration analysis of composite face sandwich plate strengthens by Al2O3 and SiO2 nanoparticles materials, *Diagnostyka,* Vol. 24, No. 2, pp. 1-9, 2023.

[6] S. Guo, X. Zhou, Free vibration analysis of multiphase reinforced resin-matrix composite shells with arbitrary boundaries and openings via back-propagation neural network algorithm, *Structures,* Vol. 80, pp. 110061, 2025/10/01/, 2025.

[7] S. Gao, R. Wang, Y. Xu, H. Zhang, S. Zhang, M. Xu, L. Liu, B. Tao, H. Xue, S. Li, B. Li, Facile construction of a micro-nano structure of green polyvinyl alcohol-based composite aerogel with superior mechanical properties, thermal insulation, and fire safety, *Polymer Degradation and Stability,* Vol. 241, pp. 111522, 2025/11/01/, 2025.

[8] D. Wang, Z. Zhang, S. Ding, C. Ning, C. Shi, Y. Ma, Q. Ren, Z. Jiang, Nano-structure and sensitivity of self-sensing geopolymer composites containing nano carbon black, *Cement and Concrete Composites,* Vol. 160, pp. 106072, 2025/07/01/, 2025.

[9] L. Zhang, H. Yuan, L. Ma, Z. Jiao, Q. Wei, Construction of TiC-TiAl3 nano-interlayer and its effect on thermo-physical properties of diamond/Al composites, *Materials Letters,* Vol. 405, pp. 139626, 2026/02/15/, 2026.

[10] M. Shishehsaz, H. Raissi, S. Moradi, Stress distribution in a five-layer circular sandwich composite plate based on the third and hyperbolic shear deformation theories, *Mechanics of Advanced Materials and Structures,* Vol. 27, No. 11, pp. 927-940, 2020/06/01, 2020.

[11] 3D free vibration analysis of nanocomposite beams carbon nanotube reinforced FGM using DQ method, *Journal of Civil Engineering Researchers,* Vol. 7, No. 2, pp. 21-37, %06/%01, 2025. en

[12] E. Kadum Njim, M. H. Al-Maamori, R. Madan, S. H. Bakhy, M. Al-Waily, P. Khobragade, L. Hadji, Numerical and Analytical Investigation of Free Vibration Behavior of Porous Functionally Graded Sandwich Plates, *Mechanics of Advanced Composite Structures,* Vol. 12, No. 3, pp. 555-568, 2025.

[13] S. Brischetto, D. Cesare, A 3D shell model for static and free vibration analysis of multilayered magneto-elastic structures, *Thin-Walled Structures,* Vol. 206, pp. 112620, 2025/01/01/, 2025.

[14] K. Djilali Djebbour, N. Mokhtar, A. A. Hassen, R. A. Alghanmi, L. Hadji, B. Riadh, An enhanced quasi-3D HSDT for free vibration analysis of porous FG-CNT beams on a new concept of orthotropic VE-foundations, *Mechanics of Advanced Materials and Structures,* Vol. 32, No. 5, pp. 893-909, 2025/03/04, 2025.

[15] A. Garg, P. Sabherwal, N. K. Shukla, L. Li, M. R. Raja, A. Sharma, R. Raman, H. D. Chalak, Free vibration analysis of laminated composite and sandwich shells using wavelet finite element method, *Mechanics of Advanced Materials and Structures,* Vol. 32, No. 11, pp. 2439-2447, 2025/06/03, 2025.

[16] K. Arshadi, M. Abasi, H. Afshari, The free vibration analysis of ring-stiffened FG conical sandwich shells with auxetic and non-auxetic honeycomb cores, *Noise & Vibration Worldwide,* Vol. 56, No. 1-2, pp. 76-97, 2025.

[17] L. Shan, C. Y. Tan, X. Shen, S. Ramesh, M. S. Zarei, R. Kolahchi, M. H. Hajmohammad, The effects of nano-additives on the mechanical, impact, vibration, and buckling/post-buckling properties of composites: A review, *Journal of Materials Research and Technology,* Vol. 24, pp. 7570-7598, 2023/05/01/, 2023.

[18] P. Zhang, Z. Wang, H. Tian, X. Xi, X. Liu, On the Magnetically Tunable Free Damped-Vibration of L-Shaped Composite Spherical Panels Made of GPL-Reinforced Magnetorheological Elastomers: An Element-Based GDQ Approach, *Thin-Walled Structures,* Vol. 218, pp. 113987, 2026/01/01/, 2026.

[19] R. A. Neamah, S. K. Al-Raheem, E. K. Njim, Z. Abboud, L. S. Al-Ansari, Experimental and Numerical Investigation of the Natural Frequency for the Intact and Cracked Laminated Composite Beam, *Journal of Aerospace Technology and Management,* Vol. 16, 2024.

[20] G. Yu, L. Peng, Y. Cheng, Morphological and mechanical relaxation characteristics of nano-SiC/crosslinked polyethylene insulation composites, *International Journal of Electrochemical Science,* Vol. 20, No. 11, pp. 101198, 2025/11/01/, 2025.

[21] K. Liu, L.-l. Xu, R. Wang, J.-L. Zhang, Y. Yuan, H. A. Mang, B. Pichler, Effect of nano-silica on material properties, pore structure, and hydration of polyacrylate/cement composite paste, *Construction and Building Materials,* Vol. 490, pp. 142503, 2025/09/05/, 2025.

[22] E. K. Njim, H. R. Hasan, M. J. Jweeg, M. Al-Waily, A. A. Hameed, A. M. Youssef, F. M. Elsayed, Mechanical Properties of Sandwiched Construction with Composite and Hybrid Core Structure, *Advances in Polymer Technology,* Vol. 2024, No. 1, pp. 3803199, 2024.

[23] F. Liu, R. Tang, Q. Li, H. Wang, Y. Zou, X. Yuan, Improved thermal performance, frost resistance, and pore structure of cement–based composites by binary modification with mPCMs/nano–SiO2, *Energy,* Vol. 332, pp. 137166, 2025/09/30/, 2025.

[24] Y. Liu, L. Zhang, Y. Yin, N. Li, X. Chu, Q. Ma, J. Liu, W. Yang, Y. Lv, S. Tao, Fabrication of composite microspheres doped with nano-aluminum powder using melt spray technology, *Chinese Journal of Chemical Engineering*, 2025/10/17/, 2025.

[25] R. Madan, P. Khobragade, E. K. Mussada, M. K. Singh, S. M. Rangappa, E. K. Njim, S. Siengchin, A novel two-step finite element approach to estimate the thermo-mechanical properties of two-phase and three-phase hybrid composites, *Composites Communications,* Vol. 53, pp. 102213, 2025/01/01/, 2025.

[26] E. Sobhani, A. R. Masoodi, A comprehensive shell approach for vibration of porous nano-enriched polymer composite coupled spheroidal-cylindrical shells, *Composite Structures,* Vol. 289, pp. 115464, 2022/06/01/, 2022.

[27] E. N. Abbas, E. Kadum Njim, M. J. Jweeg, R. Madan, A. A. F. Ogaili, F. Thair Al-Maliky, Experimental and theoretical analysis of mechanical properties of composite materials with diverse reinforcement types, *World Journal of Engineering*, 2025.

[28] C. Shi, L. Zhang, J. Zhao, L. Tian, S. Wang, X. Liu, G. Liu, Y. Shao, Characterization and performance of organic-inorganic composite zinc phosphate with nano-sheet structure synthesized by a composite reaction of sol-gel with silane modification, *Surfaces and Interfaces,* Vol. 47, pp. 104225, 2024/04/01/, 2024.

[29] P. Jankowski, K. K. Żur, Steady-state vibration of nanocomposite structures with discontinuities, *Aerospace Science and Technology,* Vol. 168, pp. 110885, 2026/01/01/, 2026.

[30] B. Saiah, M. Bachene, M. Guemana, Y. Chiker, B. Attaf, On the free vibration behavior of nanocomposite laminated plates contained piece-wise functionally graded graphene-reinforced composite plies, *Engineering Structures,* Vol. 253, pp. 113784, 2022/02/15/, 2022.

[31] Y. Abbood Mazin, S. Gill, N. Uwayed Ahmed, A. Mothanna, M. Ali, K. Njim Emad, A. Flayyih Mujtaba, R. Madan, A study of the quasi-static and low-velocity impact behavior of laminated CFRP composites, *Advances in Computational Design,* Vol. 10, No. 3, pp. 299-320, 07/25, 2025. Ko

[32] E. Sobhani, A. R. Masoodi, R. Dimitri, F. Tornabene, Free vibration of porous graphene oxide powder nano-composites assembled paraboloidal-cylindrical shells, *Composite Structures,* Vol. 304, pp. 116431, 2023/01/15/, 2023.

[33] M. Chwał, Free Vibrations and Flutter Analysis of Composite Plates Reinforced with Carbon Nanotubes, *Applied Sciences,* 15, 2025].

[34] V. N. V. Hoang, P. Shi, L. Toledo, H. Vu, Free vibration analysis of nanocomposite plate in contact with fluid using a novel quasi-3D shear deformation theory and artificial neural network, *Mechanics Based Design of Structures and Machines,* Vol. 53, No. 1, pp. 641-685, 2025/01/02, 2025.

[35] H. Yu, J. Xie, L. Yao, H. Yang, Fabrication of Microcrystalline cellulose and nano-titanium dioxide composites with broad-spectrum UV protection, *Chemical Engineering Journal,* Vol. 505, pp. 159134, 2025/02/01/, 2025.

[36] C. Chu, L. Shan, M. S. H. Al-Furjan, M. S. Zarei, M. H. Hajmohammad, R. Kolahchi, Experimental study for the effect of hole notched in fracture mechanics of GLARE and GFRP composites subjected to quasi-static loading, *Theoretical and Applied Fracture Mechanics,* Vol. 122, pp. 103624, 2022/12/01/, 2022.

[37] F. Rahmani, R. Barbaz-Isfahani, S. Saber-Samandari, M. Salehi, Experimental and analytical investigation on forced and free vibration of sandwich structures with reinforced composite faces in an acidic environment, *Heliyon,* Vol. 9, No. 10, pp. e20864, 2023/10/01/, 2023.

[38] S. Nosrati, O. Rahmani, S. A. Hosseini, Free vibration analysis of butterfly-shaped auxetic doubly curved nano-shells with nonlocal strain gradient theory, *Thin-Walled Structures,* Vol. 214, pp. 113380, 2025/09/01/, 2025.

[39] A. Noruzi, M. Mohammadimehr, F. Bargozini, Experimental and theoretical results for bending and buckling of a five-layer sandwich plate reinforced by carbon nanotubes/carbon nanorods/graphene platelets/shape memory alloy based on RFSDT, *Archive of Applied Mechanics,* Vol. 94, No. 8, pp. 2151-2173, 2024/08/01, 2024.

[40] M. Al-Waily, H. Raad, E. K. Njim, Free Vibration Analysis of Sandwich Plate-Reinforced Foam Core Adopting Micro Aluminum Powder, *Physics and Chemistry of Solid State,* Vol. 23, No. 4, pp. 659-668, 11/30, 2022.

[41] A. Kumar, R. G. Narayanan, N. Muthu, Manufacture of honeycomb core sandwich structures by hybrid approaches: Analysis using lab scale experiments and numerical simulation, *Thin-Walled Structures,* Vol. 198, pp. 111739, 2024/05/01/, 2024.

[42] A. K. Singh, R. Jaiswal, Analysis on transverse vibration of piezo-electro-magneto-thermoelastic composite nanobeams under distinct Green–Naghdi III phase lag models, *European Journal of Mechanics - A/Solids,* Vol. 113, pp. 105702, 2025/09/01/, 2025.